Clinical Neurology and Neurosurgery 261 (2026) 109277

Contents lists available at ScienceDirect

Clinical Neurology and Neurosurgery

journal homepage: www.elsevier.com/locate/clineuro

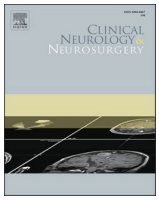

Anomaly changes in the functional connectome of post-operative neurosurgical patients: A case series

Vratko Himic [a,*], Roxanne C. Mayrand [a], Zachary C. Gersey [a], Adham M. Khalafallah [a], Victor M. Lu [a], Sima Vazquez [a], Long Di [a], Daniel M. Aaronson [a], Ashish H. Shah [a,b], Ricardo J. Komotar [a,b], Michael E. Ivan [a,b]

[a] Department of Neurological Surgery, University of Miami Miller School of Medicine, Miami, FL, USA
[b] Sylvester Comprehensive Cancer Center, University of Miami Miller School of Medicine, Miami, FL, USA

ARTICLE INFO

Keywords:
Anomaly matrix
Case series
Connectome
Correlation matrix
Neuro-oncology
Resting state fMRI

ABSTRACT

Purpose: The use of neuronavigation with superimposed mapping tools has enabled visualization of key fiber tracts and improved peri-operative planning. However, a limitation of these approaches is their reliance on a static underlying brain atlas, particularly in neurosurgical patients with brain tumors. A tool that enables qualification and quantification of brain region connectivity could refine approaches to surgical resection.
Methods: We utilized a machine learning imaging platform, Quicktome™, to generate individualized functional parcels and tracts that dynamically adapt to perioperative change. The connectome was derived from a combination of diffusion tensor imaging and resting-state function magnetic resonance imaging. Matrices were generated from the functional MRI of four patients with intracranial neoplasms and the pre- and post-operative parcellation values were compared. The individual correlation and strength of regions were quantified. Hypo- and hyper-connected regions were marked as anomalous.
Results: We present a case series of four patients to illustrate the correlation of the anomaly matrices with post-operative neurological changes. These include: post-operative delirium originating associated with salience network hypoconnectivity; visual hemineglect linked to hypoconnectivity in the dorsal attention network; and quantifiable improvements in the language network following the resolution of expressive aphasia. All differences between pre-and post-operative paired correlation values were statistically significant.
Conclusion: We demonstrate a novel approach to quantifying the extent to which anomalies in the functional connectome correlate with post-operative neurological changes. This has relevance in post-operative prognostication, provision of specialist therapy services, and could serve as a useful tool in surgical education and pre-operative planning.

1. Introduction

One of the central aims of neuro-oncological surgery is to preserve function. Advances in imaging and intra-operative monitoring have been crucial in preserving eloquent areas and their connected fiber tracts in a persistent trade-off with achieving greater tumor resection [1,2]. Previously, pre-operative planning had focused on avoiding well-defined structural features (including fiber tracts, specific gyri, and eloquent cortical regions). This approach is rooted in the early neuro-anatomical mapping concepts introduced by Brodmann in the early 20th century [3].

More recently, new mapping tools that enable peri-operative visualization and correlation of imaging with neurological function are starting to emerge [4,5]. A key limitation of such tools is their reliance on static brain atlases. While useful for cognitive research in patients with an intact parenchymal structure, these methods become less effective in neuro-oncology cases, where brain architecture is distorted. Similarly, there is a need to track these structures in the context of post-operative changes.

To address this challenge, Quicktome™, a cloud-based software platform, utilizes machine learning (ML) to generate individualized functional parcels and tracts that dynamically adapt to the perioperative change [6–8]. The personalized localization of parcellations is based on the underlying connectomic atlas [9], allowing visualization of

* Corresponding author.
E-mail address: vxh268@miami.edu (V. Himic).

https://doi.org/10.1016/j.clineuro.2025.109277
Received 11 November 2025; Accepted 26 November 2025
Available online 28 November 2025

structural changes (in the form of parcel and tractography changes) [10], as well as regional activity correlation. This is achieved through parcellation of cortical network through a combination of resting-state fMRI (rs-fMRI) and diffusion tensor imaging (DTI) tractography. Furthermore, it is possible to report anomalous connections by comparing the connections to a normative distribution from a healthy cohort. This software enhances peri-operative planning and offers insight into post-operative neurological changes.

Previous work on improving brain tumor resection has revolved around extracting data from DTI series [11–14]; however, purely relying on white matter tract data extraction can be limited by peritumoral edema and masking of tracts. The use of rs-fMRI to parcellate the brain can unlock an alternative approach. While previous reports of functional connectomic maps in neurosurgery exist [15–18], we build on this by analyzing the underlying quantifiable data that is used in their generation with a parcel-specific, network-specific approach that is clinically relevant and approachable to the treating team to analyze and use in real-time.

In this case series we illustrate the application of functional connectomic mapping through four surgical cases, demonstrating its utility in correlating function and dysfunction across specific regions (or parcellations) of the brain. We compare: (1) the difference in the paired correlation matrix values (2) the number of anomalous connections, (3) the percentage of the network exhibiting anomalies, and (4) the sum of the total anomalous connectivity values.

2. Materials and methods

2.1. Patient selection

All patients are adults being treated for intracranial lesions. Written informed consent was obtained from all patients. This study received ethical approval from our Institutional Review Board (#20200946). This case series has been reported in line with the PROCESS Guideline [19]. The patient selection process involved selecting patients with the following: full pre- and post-operative resting-state fMRI acquisitions; patients having undergone brain tumor surgery; with concomitant full neurological examination at the time of the pre- and post-operative scans. These four cases were selected for their ability to demonstrate clinical correlates of anomaly analysis in corroborating perioperative symptomatology.

2.2. Quicktome software and imaging acquisition

The Quicktome™ (Omniscient Neurotechnology Pty Ltd, Haymarket, NSW, Australia) software utilizes standard high-resolution anatomical MRI along with multi-directional diffusion tensor imaging (DTI) acquisitions to generate the Structural Connectome, allowing for parcellation and tractography-based peri-operative surgical planning. Resting-state functional MRI (rs-fMRI), which includes blood oxygen level-dependent (BOLD) sequences, is combined with DTI sequences to generate a Functional Connectome with correlation and anomaly matrices. The MRI acquisitions utilized are: multi-directional DWI, pre-contrast T1 or T2 (3D or thin slice), rs-fMRI with BOLD, and post-contrast T1, T2 and fluid-attenuated inversion recovery (FLAIR) anatomical (see Supplemental Material 1 for acquisition parameters). Pre-operative imaging was obtained within 24 hr of the surgery. Post-operative imaging was done shortly after surgery, typically post-operative day (POD) 1–4.

2.3. Image processing, data acquisition and parcellation methodology

Using rs-fMRI, functional connectivity is estimated using statistical measures (e.g., correlation, covariance) on parcel-level BOLD time-series, created by averaging voxel signals within defined brain regions. This reduces data complexity and aids in analyzing the functional connectome. Quicktome relies on anatomical parcellation before computation, using the Human Connectome Project's multi-modal atlas [7]. Each subject's brain is aligned to this atlas via topography-based registration, fitting the topography-based atlas (TbA) to underlying individual anatomy, molding around the tumor in order to trace and adhere to the confines of the gyri and sulci (see individual figures for Cases 1–4 for demonstration of this mapping around the tumor preoperatively and resection cavity post-operatively). This analysis then generates two types of data for the functional connectome: correlation and anomaly matrices. The correlation analysis evaluates the strength of individual parcel-parcel connectivity, which ranges from strong positive to strong negative correlations. The anomaly matrix highlights parcel connections that deviate significantly from expected normative patterns.

2.4. Correlation matrix generation and statistical analysis

The correlation matrix analysis represents the Pearson correlation coefficient of the BOLD times series between two brain regions (or parcels). The correlation values range from -1.00 (indicating perfect anti-correlation) to $+1.00$ (indicating perfect correlation). To assess statistically significant differences in connectivity pre- and post-operatively, a paired *t*-test was conducted at corresponding parcel-parcel connections. Hence, each connection is evaluated within the same subject, minimizing inter-subject variability. Significant differences in connectivity are identified based on a p-value threshold of $< .01$. Two-tailed paired *t*-tests were used and are reported alongside 95 % confidence intervals.

2.5. Anomaly matrix generation and statistical analysis

By contrast, anomaly matrices are generated to detect anomalously connected regions. Here, matrices are transformed using tangent space projection, allowing for comparison against a normative dataset [20]. The normative dataset consists of over 2000 subjects, from various databank sources, and has a broad age distribution and a balanced sex distribution. These have an age range of 18–42 years of age (see Supplemental Material 2 for details and dataset sources). Specific anomalies were identified based on predefined significance thresholds using z-score thresholding, which assumes a parametric distribution of connectivity values within the normative population. Following tangent space projection, each cell in the transformed matrix is assumed to follow a normal distribution, characterized by the mean and SD derived from this reference dataset. Anomaly detection is then performed by computing the z-scores for each residual value, where values exceeding ± 2 and ± 3 SD from the reference mean are flagged as anomalous, corresponding to a two-tailed p-value of approximately 0.05 and 0.003, respectively. To enhance interpretability, two threshold anomaly matrices are reported: one identifying moderate deviations exceeding ± 2 SDs, and another highlighting extreme deviation exceeding ± 3 SDs. Anomalies can be quantified as their sum or indeed as a proportion of the possible connections in that network (as a percentage of network resection). They can then be quantified on a more granular scare based on if they are hyperconnected (above the SD cut-offs) or hypoconnected (below the SD cut-offs), representing extremes in too strong of a connection or conversely too weak, respectively.

3. Results

We describe four unique cases to illustrate observable and quantifiable changes in the functional connectomic anomaly matrices, and their correlation with the patient's neurological changes (Table 1).

3.1. Case 1

A 57-year-old woman presented with a seven-year history of persistent, treatment resistant focal epilepsy. A decade prior to the onset

Table 1 –
Summary of cases with select peri-operative functional changes and the associated anomalous shifts in connection between individual relevant regions.

	Pathology	Location	Clinical correlate	Network involved	Correlation Matrix Change	Anomaly Matrix Outliers	
						±2 SD (~p < .05)	±3 SD (~p < .003)
1	Meningioma	Right temporal and parasellar	Delirium (due to capsular post-operative hemorrhage)	Salience network	0.12 ± 0.025 n = 325 connections $p = 1.63 \times 10^{-19}$	Gross global hypoconnectivity anomalies	*Areas 23c a24pr, PF, STV, PSL and FOP4
2	Astrocytoma	Right parietal	New left visual hemineglect and worse manual dexterity	Dorsal attention network	0.066 ± 0.043 n = 210 connections $p = .003$	Gross hypoconnectivity, particularly in area ‡V4t responsible for integration of visual information	§Areas PFt with AIP – grasping objects under visual guidance
3	Astrocytoma	Left parasagittal parietal	New post-operative lower limb weakness	Sensorimotor network	0.16 ± 0.047 n = 78 connections $p = 4.77 \times 10^{-9}$	Hypoconnectivity in anterior cingulate regions responsible for lower limb movement initiation and planning	None meeting 3 SD threshold
4	Glioblastoma	Left tempo-parietal	Improvement of preoperative expressive aphasia	Language network	0.045 ± 0.026 n = 276 connections $p = .0009$	Reduction in hypoconnectivity in Broca's complex and hyperconnectivity in the medial belt	#Resolution of pre-operative MBelt anomaly

Case 1 demonstrates a large increase in hypoconnectivity anomalies post-operatively at the 2 SD threshold. *At the 3 SD threshold, notable anomaly pairings include areas 23c, a24pr, PF (parietal area F), STV (superior temporal visual area), PSL (perisylvian language area) and FOP4 (frontal operculum 4). Together these areas have been implicated in higher cognitive functions such as essential information processing, emotional and cognitive control, and actions that require an external focus. In Case 2, the 2 SD anomaly threshold reveals new ‡V4t (visual area 4) hypoconnectivity; V4t integrates dorsal and ventral visual stream information. At the 3 SD threshold, §areas PFt (parietal area F, part t) and AIP (anterior intraparietal) are anomalous; both responsible for coordinating grasping actions under visual guidance. In Case 4, #we see a resolution of the pre-operative hyperconnectivity anomaly between MBelt (medial belt of the parietal apex) and STSvp (superior temporal sulcus ventral posterior), which display a role in language comprehension and auditory story tasks.

of epilepsy she underwent resection of a right temporal and parasellar meningioma. At presentation, she was maintained on lamotrigine and topiramate and was neurologically intact with a normal neuro-cognitive pre-operative baseline. She subsequently underwent a right temporal partial lobectomy and resection of the lesion, with pathology confirming a CNS WHO Grade 1 meningioma (Figs. 1, 1**a-e**). Her immediate post-operative course was complicated by a large temporal hemorrhage due to a temporal lobe venous infarction at the resection cavity leading to a prolonged post-operative stay in the intensive care unit with hyperactive delirium and agitation. This was corroborated by a reduction in the correlation matrix values in the salience network post-operatively; mean reduction of 0.121 [95 %CI: 0.097–0.146], n = 325 connections, $p = 1.62 \times 10^{-19}$ (Figs. 1, 1**f-g**). The anomaly matrix also demonstrated significant global hypoconnectivity in the salience network post-operatively, compared to being relatively intact pre-operatively. At 2 SD, the sum of hypoconnected anomalies was more negative post-operatively (from −0.32 to −4.41) (Figs. 1, 1**h**, 1**j**). The proportion of the salience network that was anomalous increased postoperatively (from 2.15 % to 8.31 %). Post-operatively, three connections surpassed the 3 SD anomaly threshold, all involving parcellations that have been implicated in higher cognitive functions such as essential information processing, emotional and cognitive control, and actions that require an external focus (Figs. 1, 1**i**). She has since recovered well, with a reassuring post-operative scan.

3.2. Case 2

This 38-year-old woman with a history of resection and adjuvant chemotherapy for right parieto-occipital high-grade glioma presented to our service after radiographic progression of the disease. She was experiencing persistent headaches, subacute progressive paresthesias in the left hemibody, and an episode of left involuntary arm movement. She underwent a right parietal redo craniotomy for tumor resection (Figs. 2, 2**a-e**), and pathology confirmed IDH-mutant astrocytoma with MGMT methylation and ATRX loss. Post-operatively, she developed new left-sided hemineglect. Analysis of the dorsal attention network, a network crucial for focusing attention on externally directed tasks while filtering out miscellaneous noises or environmental changes, revealed global reduction in parcel-parcel correlation and new anomalous hypoconnectivity post-operatively. The post-operative correlation matrix mean was reduced by 0.066 [95 %CI: 0.023–0.11], n = 210 connections, p = .003 (Figs. 2, 2**f-g**). Post-operative anomalies at the 2 SD cut-off demonstrated significant hypoconnectivity post-operatively (-0.15 to −2.23) (Figs. 2, 2**h**, 2**j**) and increased anomaly proportion (1.9–7.14 %). Notably, the new hemineglect correlated with new anomalous hypoconnectivity of Area V4t, a region on the lateral occipital surface that integrates visual information from the dorsal and ventral visual streams and processes shape-sensitive and global motion information. On 3 SD anomaly review, one hypoconnected area remained between areas PFt and API (Figs. 2, 2**i**). Together these areas coordinate grasping under visual guidance. Her post-operative course was complicated by multiple re-admissions due to breakthrough seizures. She is currently maintained on levetiracetam and dexamethasone without further seizures.

3.3. Case 3

A 39-year-old woman presented with lower extremity numbness and a lesion in the left parasagittal frontoparietal lobe, 2.3 × 3.8 cm in size and with central necrosis and peripheral enhancement (Figs. 3, 3**a-f**). After thorough intraoperative monitoring, maximal safe resection was achieved, with multiple positive areas around the tumor mapping positive during awake motor mapping. Pathology revealed a diffuse IDH-mutant astrocytoma (grade 3). Immediately post-operatively, she developed right lower limb weakness with 3–4/5 power, along with persistent right lower limb paresthesia. The sensorimotor network correlation matrix demonstrated a post-operative mean reduction of 0.156 [95 %CI: 0.109–0.203], n = 78 connections, $p = 4.77 \times 10^{-9}$ (Figs. 3, 3**g-h**). Analysis of her sensorimotor network 2 SD anomaly matrices revealed dynamic changes; post-operative anomalies were more negative (-0.38 to −0.51) whilst pre-operative hyperconnections normalized (Figs. 3, 3**i**, 3**k**). Particularly relevant in the context of her new lower limb weakness was new anomalous hypoconnectivity of Area 24dd at 2 SD, a region of the anterior cingulate cortex involved in the initiation and planning of lower limb movements; this region accounted for 61 % of all post-operative anomalous 2 SD values. A review of her pre-operative structural connectome revealed a bundle of fibers from Area 24dd enveloping the lesion postero-superiorly (Figs. 3, 3**c**). Post-

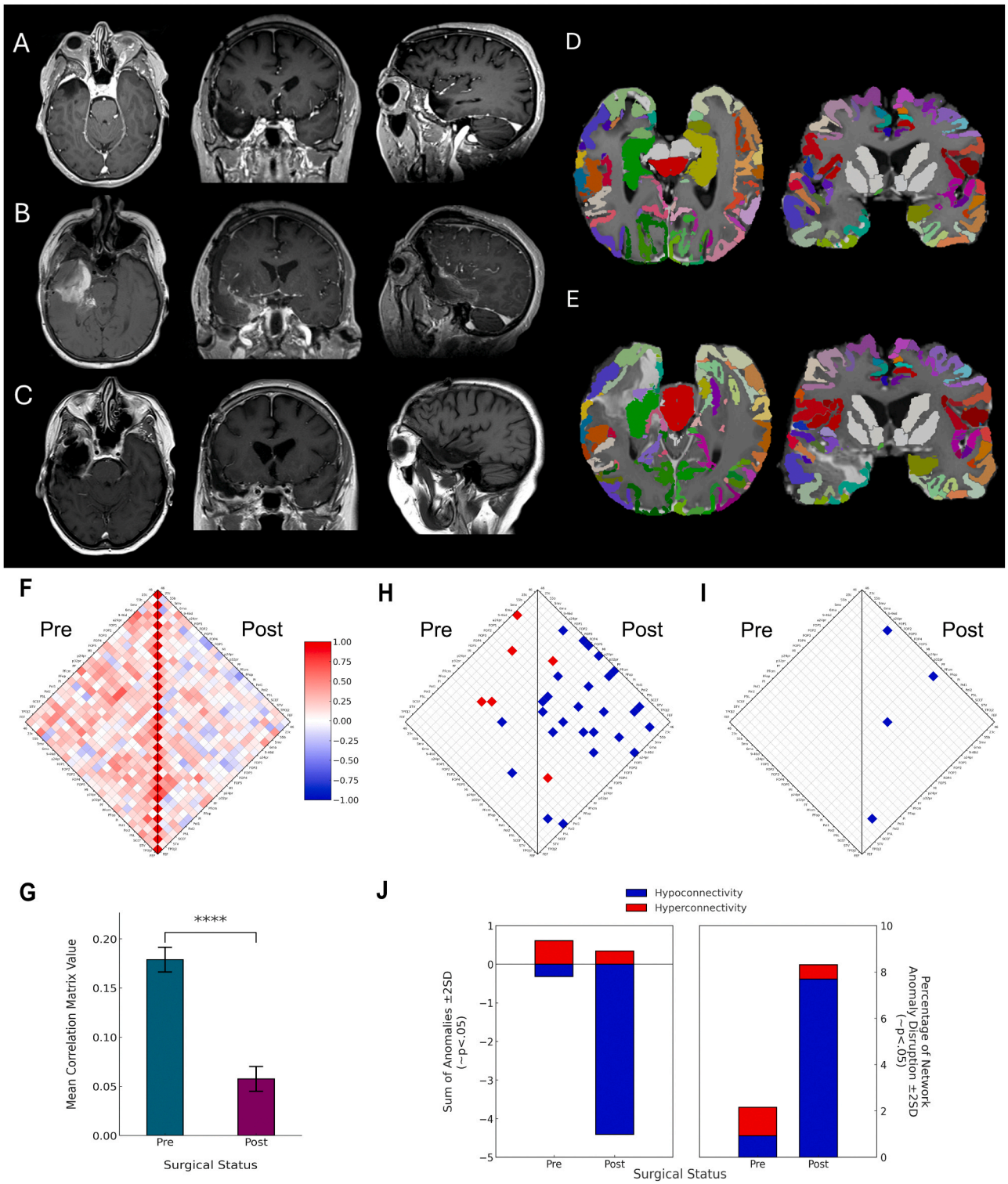

Fig. 1. A-E: Imaging for Case 1 demonstrating a right temporal, parasellar meningioma. Top Row (A) Pre-operative MR T1 with contrast image. Middle Row (B) Axial MR T1 without contrast showing resection cavity hemorrhage and coronal and sagittal MR T1 with contrast images showing the mass effect. Taken on postoperative day 10. Bottom Row (C) Six-month follow-up MR T1 with contrast images showing resolution and sagittal MR T1 without contrast. D – Pre-operative connectome overlay of connectome atlas, with the fitted topography-based atlas in patient coordinate space, comparable to the HCP-MMP 1.0 atlas. E – Post-operative connectome overlay of the topography-based atlas. F-J: A comparison of the pre- and post-operative correlation and anomaly matrices of the functional connectome of the right salience network for Case 1. F – correlation matrix compared pre- and post-operatively. G – bar chart comparing pre- and post-operative means of the correlation matrix values with means difference standard error (two-tailed paired *t*-test). H – 2 SD anomaly matrix compared pre- and post-operatively. I - 3 SD anomaly matrix compared pre- and post-operatively. J – bar charts showing the sum of anomaly values comparison (left) and the percentage of network anomaly disruption comparison (right). NB: *The matrices display the pre-operative matrix on the left side and post-operative matrix on the right. In the correlation matrix, strength of correlation (or anti-correlation) is displayed in a red to blue gradient representing (+1 to −1). In the anomaly matrix, each value that is either blue (hypoconnected) or red (hyperconnected) is significantly different from other connections to ±2 or ±3 SD. 2 SD: two standard deviations; 3 SD – three standard deviations.*

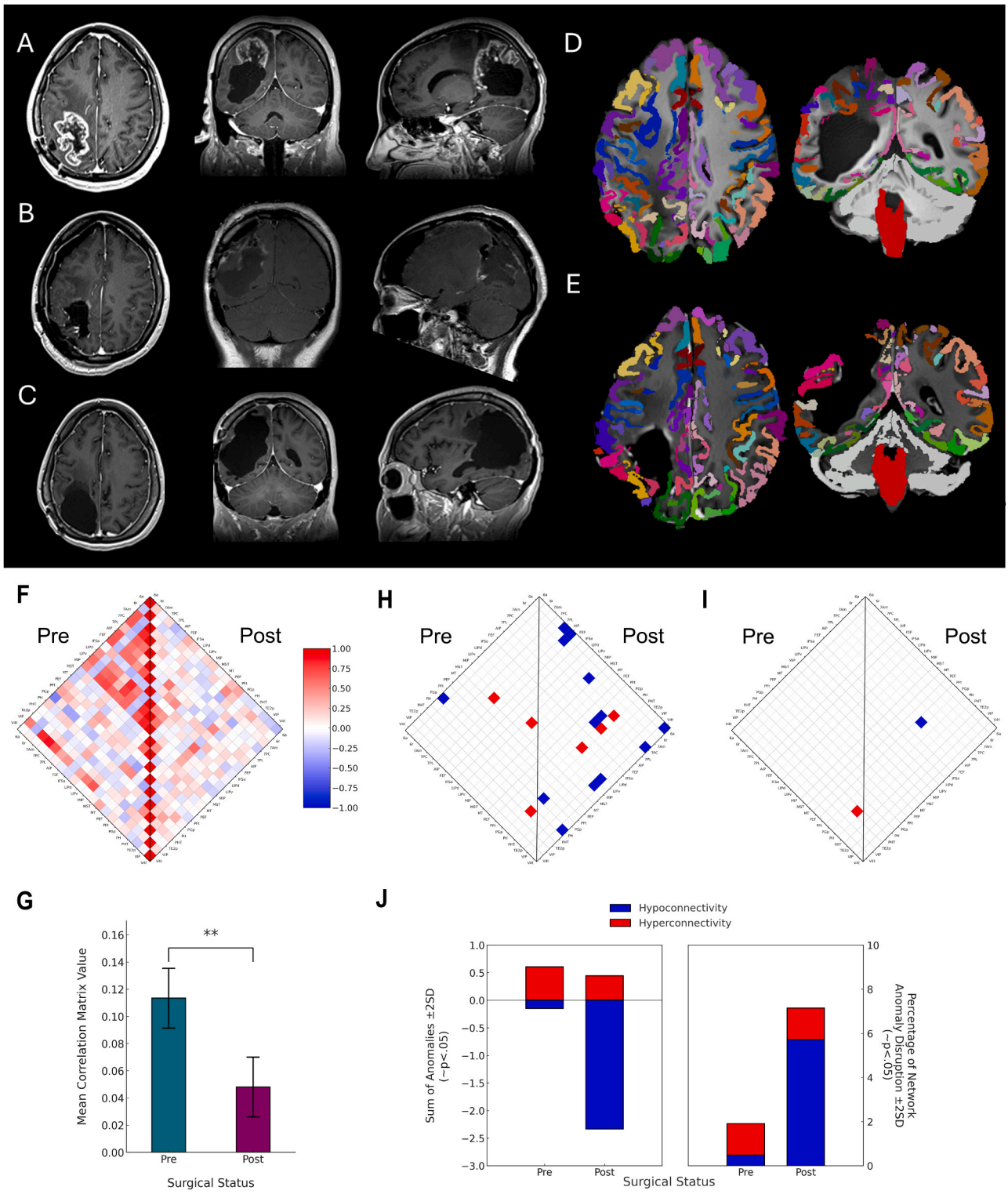

Fig. 2. A-E: Imaging for Case 2 demonstrating a right parieto-occipital astrocytoma. Top Row (A) Pre-operative MR T1 with contrast. Middle Row (B) Post-operative MR T1 with contrast taken at post-operative day 1. Bottom Row (C) 13-month follow-up MR T1 with contrast images. D – Pre-operative connectome overlay of connectome atlas, with the fitted topography-based atlas in patient coordinate space, comparable to the HCP-MMP 1.0 atlas. E – Post-operative connectome overlay of the topography-based atlas. F-J: A comparison of the pre- and post-operative correlation and anomaly matrices of the functional connectome of the right dorsal attention network for Case 2. F – correlation matrix compared pre- and post-operatively. G – bar chart comparing pre- and post-operative means of the correlation matrix values with means difference standard error (two-tailed paired *t*-test). H – 2 SD anomaly matrix compared pre- and post-operatively. I - 3 SD anomaly matrix compared pre- and post-operatively. J – bar charts showing the sum of anomaly values comparison (left) and the percentage of network anomaly disruption comparison (right). NB: *The matrices display the pre-operative matrix on the left side and post-operative matrix on the right. In the correlation matrix, strength of correlation (or anti-correlation) is displayed in a red to blue gradient representing (+1 to −1). In the anomaly matrix, each value that is either blue (hypoconnected) or red (hyper-connected) is significantly different from other connections to ±2 or ±3 SD. 2 SD: two standard deviations; 3 SD – three standard deviations.*

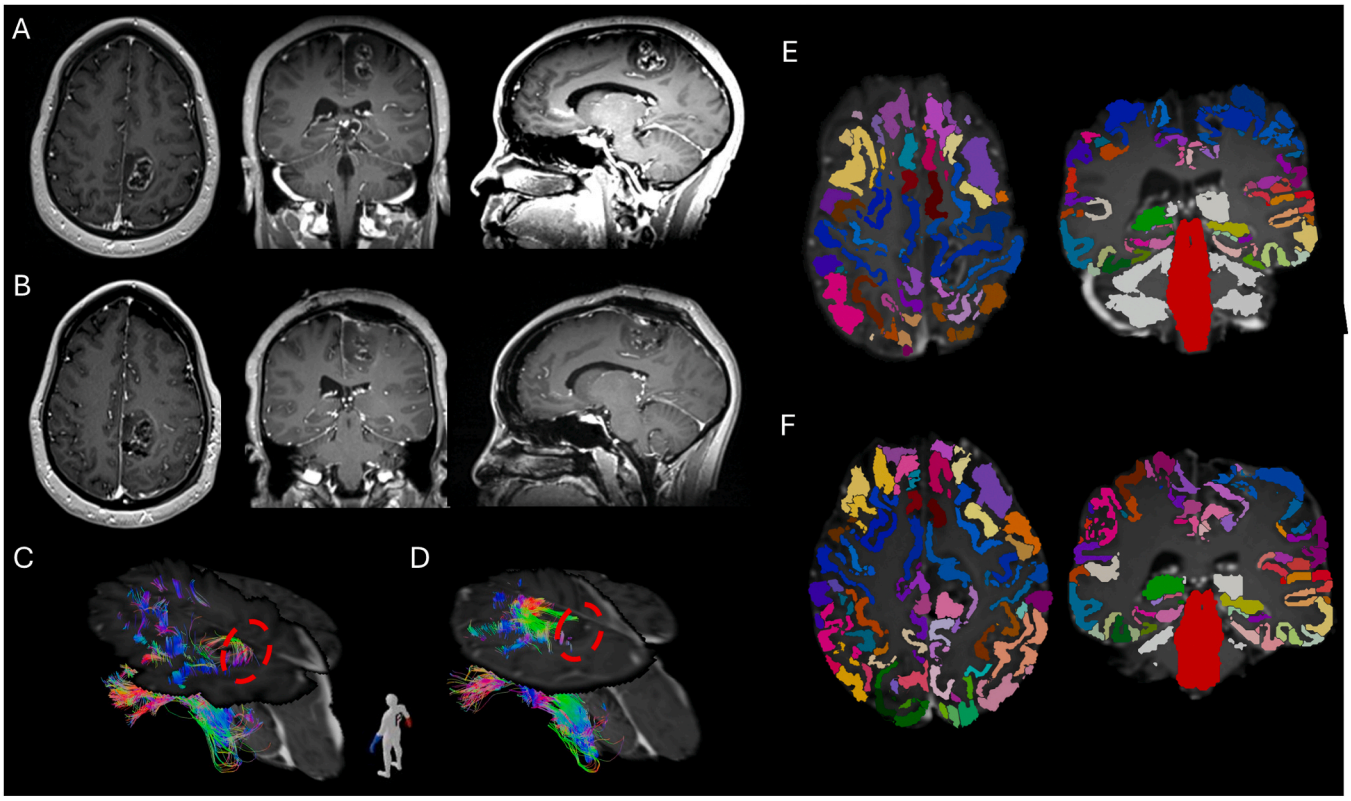

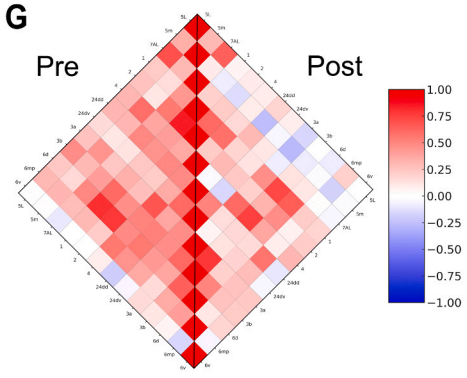

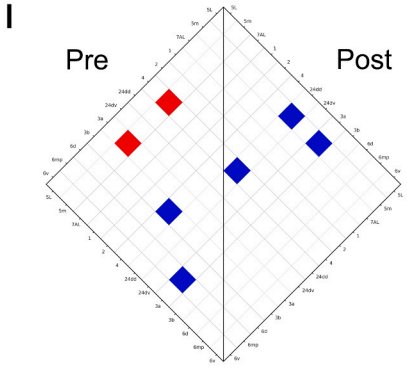

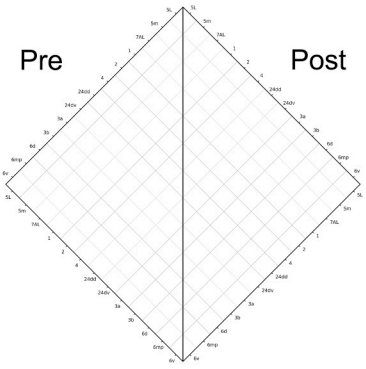

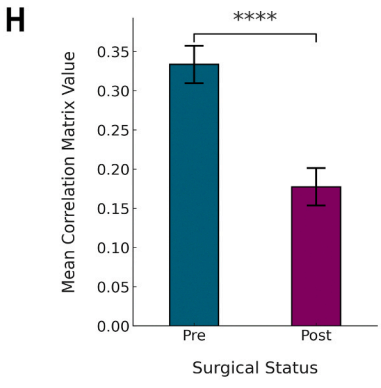

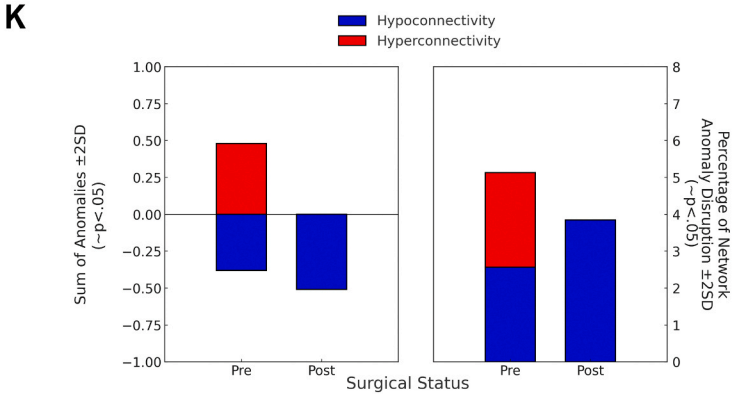

(caption on next page)

Fig. 3. A-F: Imaging for Case 3 demonstrating a left parasagittal parietal diffuse astrocytoma. A, Top Row: Pre-operative MR T1 with contrast images. B, Middle row: Post-operative MR T1 with contrast taken at post-operative day 1 with maximal safe resection achieved. Bottom row: (C) pre-operative structural connectome showing the left corticospinal tract in a 3D view from latero-superior-posterior view (see orientation of mannequin). The red-dashed circle demonstrates the posteriorly-arching fibers of areas 24dd around the tumor just anterior and (D) their loss post-operatively, correlating with the changes in the anomaly matrices. E – Pre-operative connectome overlay of connectome atlas, with the fitted topography-based atlas in patient coordinate space, comparable to the HCP-MMP 1.0 atlas. F – Post-operative connectome overlay of the topography-based atlas. G-K: A comparison of the pre- and post-operative correlation and anomaly matrices of the functional connectome of the left sensorimotor network for Case 3. G – correlation matrix compared pre- and post-operatively. H – bar chart comparing pre- and post-operative means of the correlation matrix values with means difference standard error (two-tailed paired *t*-test). I – 2 SD anomaly matrix compared pre- and post-operatively. J - 3 SD anomaly matrix compared pre- and post-operatively. K – bar charts showing the sum of anomaly values comparison (left) and the percentage of network anomaly disruption comparison (right). NB: *The matrices display the pre-operative matrix on the left side and post-operative matrix on the right. In the correlation matrix, strength of correlation (or anti-correlation) is displayed in a red to blue gradient representing (+1 to −1). In the anomaly matrix, each value that is either blue (hypoconnected) or red (hyperconnected) is significantly different from other connections to ±2 or ±3 SD. 2 SD: two standard deviations; 3 SD – three standard deviations.*

operatively, this bundle of fibers was lost (Figs. 3, 3**d**). No anomalies reached the 3 SD threshold pre- or post-operatively in the sensorimotor network (Figs. 3, 3**j**). The patient is now undergoing rehabilitation for her new limb weakness.

3.4. Case 4

An 81-year-old man presented with several weeks of mild confusion, lethargy, and mild expressive aphasia. Imaging revealed an enhancing, necrotic, and partially hemorrhagic left temporoparietal mass with surrounding edema, concerning for high-grade glioma (Figs. 4, 4**a-d**). It involved eloquent language areas, and pathology confirmed glioblastoma. Post-operatively his speech improved, and he was more alert and conversant. This improvement was also reflected in the anomaly matrices of the language network. At the 2 SD threshold, there was global anomaly reduction post-operatively and less of the network was disrupted (Figs. 4, 4**g**, 4**h**). Particularly pertinent are the reductions in anomalous connections in areas 44 and 45 (Broca's complex). Area 44 is responsible for translating abstract and intentional information in the prefrontal area to guide verbal and manual actions. Furthermore, there was a total resolution of the four anomalously hyperconnected regions of the medial belt (MBelt) area postoperatively. In the 3 SD anomaly view, the previously extreme outlier anomaly between the MBelt and STSvp resolved post-operatively (Figs. 4, 4**i**). The MBelt is a relatively new parcellation of the auditory cortex involved in arithmetic and auditory story tasks. By contrast, whilst the hearing function improved modestly post-operatively, there was a reduction in the mean correlation matrix post-operatively; mean difference of 0.045 [95 %CI: 0.018–0.071], n = 276 connections, p = .0009 (Figs. 4, 4**e-f**). He was discharged with resolved aphasia, without confusion and with intact power and sensation.

4. Discussion

Integrating functional connectomic imaging into clinical practice has the potential to aid in visualizing and quantifying peri-operative neurological changes. When combined with the structural connectome, this technology supports a patient-specific approach to pre-operative planning, particularly in preserving neurological function while maximizing the extent of safe resection. Importantly, this can now be done at the resolution of individual parcellations.

In this case series, we demonstrate a novel quantification analysis of correlations and anomalous connections between individual regions using Quicktome™. Previous case series have demonstrated structural and functional tractography maps, including their use as a prognostic tool in glioma surgery [16] and intra-operative awake language mapping [15]. Building upon these findings, we provide quantifiable measures that determine not only the extent of network correlation, but also assess individual connection anomalies, going beyond a binary read-out.

Each case highlights a different interpretation of the anomaly changes. Case 1 illustrates global neurocognitive dysfunction due to a post-operative bleed leading to widespread hypoconnectivity anomalies (both in their sum and as a percentage of the total salience network) [21]. Case 2 extends this concept, demonstrating hypoconnectivity in the dorsal attention network [22–24], while also identifying anomalous connections of area V4t, a crucial region for visual information integration, correlating with the patient's new left-sided hemineglect [25–27]. At the 3 SD anomaly cut-off, this patient's worsened performance in the pegboard test is underscored by the extreme hypoconnectivity between regions PFt and AIP, together responsible for grasping activity under visual guidance. These findings suggest that network-level and region-specific anomalies can directly correlate with new neurologic dysfunction. Case 3 underscores the importance of pre-operative structural connectome review in predicting post-operative functional changes. Here, the patient's post-operative lower limb weakness corresponded to hypoconnectivity in area 24dd, a key region for lower limb motor planning [28,29]. A retrospective analysis of the pre-operative structural connectome revealed that the fibers that were lost post-operatively were indeed those associated with this area. Lastly, Case 4 demonstrates a more nuanced interpretation, where mild expressive aphasia showed partial postoperative resolution, reflected in the anomaly matrices trending toward non-anomalous values [30–32]. Despite mixed hypo- and hyperconnectivity patterns, the sum of these anomalous values trends towards 0 postoperatively, suggesting a return to non-anomalous activity.

However, Case 4 also demonstrates the different interpretations of the correlation and anomaly matrices. In this case, whilst the hearing improved post-operatively, there was a mean reduction in the correlation post-operatively; this differs from the observations in Cases 1–3 where a worsening in the anomaly matrix postoperatively is associated with a mean decrease in correlation in a network. However, it is important to note that a network being more or less correlated (trending further from 0) does not necessarily mean aberrant correlation; it informs us that there is a real intra-subject difference post-operatively. By contrast, the power of the anomaly matrix is its ability to contextualize these signal changes by comparing the data to connectivity matrices derived from a healthy reference dataset. In this way, the correlation matrix reveals quantifiable activity changes that are statistically significant, whereas the anomaly matrix demonstrates clinically relevant outliers that are significant (2 SD) or very significantly (3 SD) above or below the expected parcel-parcel connectivity.

Regarding previous efforts to quantify the output of the functional connectome in the form of functional network/whole-brain connectivity (FC), these have centered around comparing network features such as centrality and resilience with neurocognitive outcomes [33], modularity, clustering coefficient and efficiency with neuropsychological outcomes [34], and FC alongside tumor location to predict functional outcomes based on KPS [35]. While these approaches generate a well-quantified FC measure, when compared to the approach deployed in our work through Quicktome™, they do not delineate whether a parcel-parcel connection or indeed network activity is "abnormal" or "anomalous". These anomaly matrices enable a clinically relevant and more easily interpretable read-out which, through the software portal of Quicktome™ allows rapid and real time pre-surgical planning and peri-operative decision making.

Other groups have also gone on to define "abnormality" through a

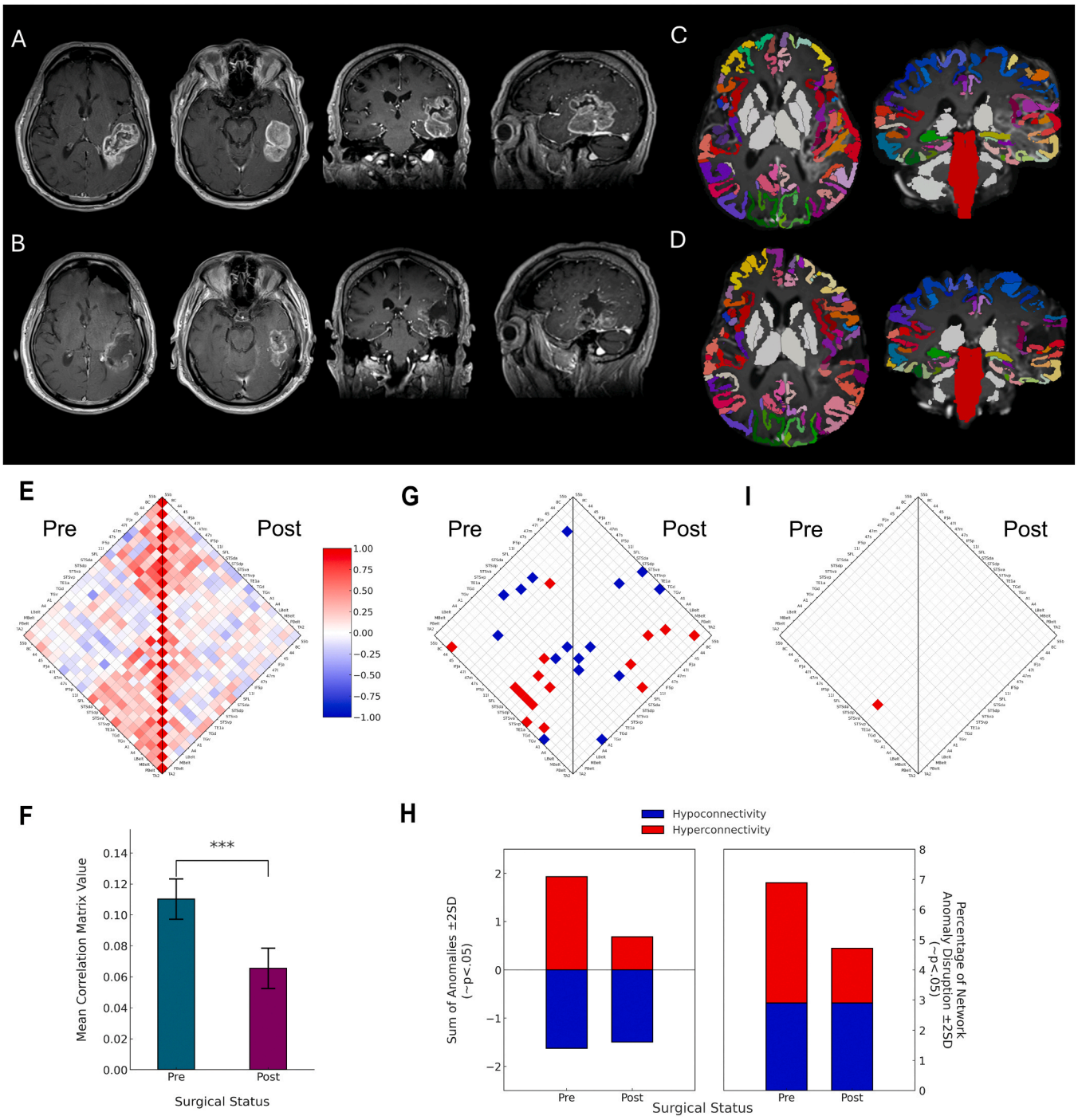

Fig. 4. A-D: Imaging for Case 4 demonstrating a left temporo-parietal glioblastoma involving the eloquent language areas. A: Pre-operative MR T1 with contrast image with two axial slices (one more cranial, one more caudal). B: Post-operative MR T1 with contrast taken at post-operative day 1 with maximal safe resection achieved, again with two axial slices (one more cranial, one more caudal). C – Pre-operative connectome overlay of connectome atlas, with the fitted topography-based atlas in patient coordinate space, comparable to the HCP-MMP 1.0 atlas. D – Post-operative connectome overlay of the topography-based atlas. E-H: A comparison of the pre- and post-operative correlation and anomaly matrices of the functional connectome of the language network for Case 4. E – correlation matrix compared pre- and post-operatively. F – bar chart comparing pre- and post-operative means of the correlation matrix values with means difference standard error (two-tailed paired *t*-test). G – 2 SD anomaly matrix compared pre- and post-operatively. H – bar charts showing the sum of anomaly values comparison (left) and the percentage of network anomaly disruption comparison (right). I - 3 SD anomaly matrix compared pre- and post-operatively. NB: *The matrices display the pre-operative matrix on the left side and post-operative matrix on the right. In the correlation matrix, strength of correlation (or anti-correlation) is displayed in a red to blue gradient representing (+1 to −1). In the anomaly matrix, each value that is either blue (hypoconnected) or red (hyperconnected) is significantly different from other connections to ±2 or ±3 SD. 2 SD: two standard deviations; 3 SD – three standard deviations.*

form of anomaly analysis. Stoecklein and colleagues deployed rs-fMRI to calculate an abnormality index by comparing FC data to the Genomics Superstruct Project sample of 1000 healthy subjects; they report that connectomic abnormalities can be seen within the lesional tissue as well as in healthy tissue and that aggressivity (as defined by WHO grade), as well as IDH1 status were associated with abnormal connectivity [36]. This approach, however, does not allow for parcel-parcel specific analysis of anomalies that can be used to directly correlate to patient-specific outcomes in their neurological exam or across neurocognitive domains. Of note, Nenning and colleagues reported on a cohort of GBM patients that underwent rs-fMRI data and generated anomaly analysis that showed that the functional proximity (rather than anatomical spatial distance) of tumor to the network was associated with greater network disruption [37]. In this case, whilst the anomalies and voxels were stratified into specific networks, the reference cohort was composed of only 80 control patients (compared to the 2011 reference scans in Quicktome™). Given the cut-offs used to define something as truly "anomalous", which in the case of our anomaly analysis is set at least 2 SD or 3 SD, a large reference healthy data set with a balanced sex and age distribution is key.

4.1. Limitations

One limitation of this study is that pre- and post-operative scans provide only a single snapshot, without capturing long-term dynamic changes. To address this, we are conducting six-month follow-up scans to track evolving functional changes. This will help determine whether anomaly changes are transient, particularly in cases involving hemorrhage or midline shift, or if persistent signals remain as biomarkers of a resolved neurological deficit. Another challenge in this current workflow is the retrospective nature of network analysis, where clinical symptoms guide the identification of affected networks and their contributing parcels. While the anomaly maps rank parcellations from "most" to "least" anomalous, functional deficits do not always have direct anomaly correlates, particularly in cases with less severe or clinically elicitable symptoms. Thus, reproducible and reliable clinical neurological examination remains essential, serving as a foundation for retrospectively correlating the imaging. This will be particularly useful in the pre-operative planning stage, allowing for prospective identification of tracts at risk and guiding surgical decision-making for future cases.

4.2. Clinical implications and future directions

Interpretation of the quantified pre- and post-operative correlation and anomaly matrices has both short-term and longer-term clinical implications. In the short-term, matrix data of this kind can help complement and refine existing functional preservation techniques including intraoperative neurophysiology and awake mapping. Pre-operatively, it is possible to superimpose the connectomic tractography onto the patient intraoperatively using augmented reality headsets [38].

In the longer-term, post-operative anomalous changes could be used to predict patient outcomes and tailor post-operative speech and physical therapy. This technology could play a critical role in understanding neurocognitive changes beyond motor and language deficits. Post-operative changes in mood, memory, and cognition remain underappreciated in neurosurgical care, yet they have a profound impact on quality of life. Targeted neuropsychiatric testing combined with connectomic imaging may provide new insights into these higher-order functional changes [39–41].

To strengthen this use-case in the long-term, larger prospective study cohorts are needed to validate these findings. In addition, due to the relative complexity of interpreting the correlation matrix changes, virtual brain network analysis [42] as well as new machine-learning models could be deployed to clarify the extent to which regional and focal connectomic changes make a tangible difference in the long-term outcomes of patients.

CRediT authorship contribution statement

Mayrand Roxanne: Data curation, Formal analysis, Methodology, Project administration, Writing – review & editing. **Vratko Himic:** Conceptualization, Data curation, Formal analysis, Investigation, Methodology, Project administration, Validation, Visualization, Writing – original draft, Writing – review & editing. **Ivan Michael E:** Funding acquisition, Investigation, Project administration, Resources, Software, Supervision, Validation, Visualization, Writing – review & editing. **Komotar Ricardo J:** Investigation, Project administration, Resources, Supervision, Writing – review & editing. **Shah Ashish H:** Investigation, Supervision, Writing – review & editing. **Aaronson Daniel M:** Conceptualization, Investigation, Supervision, Writing – review & editing. **Long Di:** Project administration, Supervision, Writing – review & editing. **Sima Vazquez:** Data curation, Project administration, Resources, Writing – review & editing. **Lu Victor M:** Supervision, Writing – original draft, Writing – review & editing. **Khalafallah Adham M:** Supervision, Writing – original draft, Writing – review & editing. **Gersey Zachary C:** Supervision, Writing – original draft, Writing – review & editing.

Acknowledgments

The authors would like to sincerely thank StacheStrong for their generous financial support of this research project. Omniscient Neurotechnology. Quicktome [software]. Sydney, Australia: Omniscient Neurotechnology; Available from: https://www.o8t.com/quicktome.

Financial disclosures

This work was supported by StacheStrong. Dr Michael E. Ivan is a consultant for Omniscient Neurotechnology.

Appendix A. Supporting information

Supplementary data associated with this article can be found in the online version at doi:10.1016/j.clineuro.2025.109277.

References

[1] J.K. Tabor, D. Bonda, B.C. LeMonda, R.S. D'Amico, Neuropsychological outcomes following supratotal resection for high-grade glioma: a review, J. Neurooncol. 152 (2021).
[2] S.L. Hervey-Jumper, M.S. Berger, Evidence for improving outcome through extent of resection, Neurosurg. Clin. N. Am. 30 (2019).
[3] K. Zilles, Brodmann: a pioneer of human brain mapping-His impact on concepts of cortical organization, Brain 141 (2018).
[4] P. Unadkat, L. Fumagalli, L. Rigolo, et al., Functional MRI task comparison for language mapping in neurosurgical patients, J. Neuroimaging 29 (2019), https://doi.org/10.1111/jon.12597.
[5] V.A. Kumar, I.M. Heiba, S.S. Prabhu, et al., The role of resting-state functional MRI for clinical preoperative language mapping, Cancer Imaging 20 (2020), https://doi.org/10.1186/s40644-020-00327-w.
[6] J.D. Tournier, C.H. Yeh, F. Calamante, et al., Resolving crossing fibres using constrained spherical deconvolution: Validation using diffusion-weighted imaging phantom data, Neuroimage 42 (2008), https://doi.org/10.1016/j.neuroimage.2008.05.002.
[7] M.F. Glasser, T.S. Coalson, E.C. Robinson, et al., A multi-modal parcellation of human cerebral cortex, Nature 536 (2016), https://doi.org/10.1038/nature18933.
[8] S. Doyen, P. Nicholas, A. Poologaindran, et al., Connectivity-based parcellation of normal and anatomically distorted human cerebral cortex, Hum. Brain Mapp. 43 (2022), https://doi.org/10.1002/hbm.25728.
[9] C.M. Baker, J.D. Burks, R.G. Briggs, et al., A connectomic atlas of the human cerebrum-chapter 1: introduction, methods, and significance, Oper. Neurosurg. 15 (2018), https://doi.org/10.1093/ons/opy253.
[10] A.A. Morell, D.G. Eichberg, A.H. Shah, et al., Using machine learning to evaluate large-scale brain networks in patients with brain tumors: traditional and non-traditional eloquent areas, Neurooncol Adv. 4 (2022), https://doi.org/10.1093/noajnl/vdac142.

[11] M. Zoli, L. Talozzi, M. Martinoni, et al., From neurosurgical planning to histopathological brain tumor characterization: potentialities of arcuate fasciculus along-tract diffusion tensor imaging tractography measures, Front. Neurol. 12 (2021), https://doi.org/10.3389/fneur.2021.633209.
[12] V. Pieri, F. Sanvito, M. Riva, et al., Along-tract statistics of neurite orientation dispersion and density imaging diffusion metrics to enhance <scp>MR</scp> tractography quantitative analysis in healthy controls and in patients with brain tumors, Hum. Brain Mapp. 42 (2021) 1268–1286, https://doi.org/10.1002/hbm.25291.
[13] M. Chamberland, S. Genc, C.M.W. Tax, et al., Detecting microstructural deviations in individuals with deep diffusion MRI tractometry, Nat. Comput. Sci. 1 (2021) 598–606, https://doi.org/10.1038/s43588-021-00126-8.
[14] Y. Wei, C. Li, Z. Cui, et al., Structural connectome quantifies tumour invasion and predicts survival in glioblastoma patients, Brain 146 (2023) 1714–1727, https://doi.org/10.1093/brain/awac360.
[15] H.A. Shah, F. Ablyazova, A. Alrez, et al., Intraoperative awake language mapping correlates to preoperative connectomics imaging: an instructive case, Clin. Neurol. Neurosurg. 229 (2023), https://doi.org/10.1016/j.clineuro.2023.107751.
[16] E.S. Molina, M.J. Tait, A. Di Ieva, Connectomics as a prognostic tool of functional outcome in glioma surgery of the supplementary motor area: illustrative case, J. Neurosurg. Case Lessons 6 (2023), https://doi.org/10.3171/CASE23286.
[17] M. Magnani, A. Rustici, M. Zoli, et al., Connectome-based neurosurgery in primary intra-axial neoplasms: beyond the traditional modular conception of brain architecture for the preservation of major neurological domains and higher-order cognitive functions, Life 14 (2024).
[18] B.K. Hendricks, L. Scherschinski, J.H. Jubran, et al., Eloquent noneloquence: redefinition of cortical eloquence based on outcomes of superficial cerebral cavernous malformation resection, J. Neurosurg. 141 (2024), https://doi.org/10.3171/2023.12.JNS232588.
[19] G. Mathew, C. Sohrabi, T. Franchi, et al., Preferred reporting of case series in surgery (PROCESS) 2023 guidelines, Int. J. Surg. (2023), https://doi.org/10.1097/JS9.0000000000000940.
[20] K. Dadi, M. Rahim, A. Abraham, et al., Benchmarking functional connectome-based predictive models for resting-state fMRI, Neuroimage 192 (2019), https://doi.org/10.1016/j.neuroimage.2019.02.062.
[21] V. Menon, Salience Network. Brain Mapping, Elsevier, 2015, pp. 597–611.
[22] H.O. Karnath, Spatial attention systems in spatial neglect, Neuropsychologia 75 (2015).
[23] A.M. Barrett, O. Boukrina, S. Saleh, Ventral attention and motor network connectivity is relevant to functional impairment in spatial neglect after right brain stroke, Brain Cogn. 129 (2019), https://doi.org/10.1016/j.bandc.2018.11.013.
[24] M. Corbetta, G.L. Shulman, Spatial neglect and attention networks, Annu Rev. Neurosci. 34 (2011), https://doi.org/10.1146/annurev-neuro-061010-113731.
[25] A.W. Roe, L. Chelazzi, C.E. Connor, et al., Toward a unified theory of visual area V4, Neuron 74 (2012).
[26] C.E. Connor, Active vision and visual activation in area V4, Neuron 40 (2003).
[27] A. Pasupathy, D.V. Popovkina, T. Kim, Visual functions of primate area V4, Annu Rev. Vis. Sci. 6 (2020).
[28] D.S. Margulies, A.M.C. Kelly, L.Q. Uddin, et al., Mapping the functional connectivity of anterior cingulate cortex, Neuroimage 37 (2007), https://doi.org/10.1016/j.neuroimage.2007.05.019.
[29] I. Oane, A. Barborica, F. Chetan, et al., Cingulate cortex function and multi-modal connectivity mapped using intracranial stimulation, Neuroimage 220 (2020), https://doi.org/10.1016/j.neuroimage.2020.117059.
[30] E. Fedorenko, J. Duncan, N. Kanwisher, Language-selective and domain-general regions lie side by side within Broca's area, Curr. Biol. 22 (2012), https://doi.org/10.1016/j.cub.2012.09.011.
[31] D. Saura, B.W. Kreher, S. Schnell, et al., Ventral and dorsal pathways for language, Proc. Natl. Acad. Sci. USA 105 (2008), https://doi.org/10.1073/pnas.0805234105.
[32] C.J. Price, A review and synthesis of the first 20years of PET and fMRI studies of heard speech, spoken language and reading, Neuroimage 62 (2012).
[33] K.R. Noll, H.S. Chen, J.S. Wefel, et al., Alterations in functional connectomics associated with neurocognitive changes following glioma resection, Neurosurgery 88 (2021) 544–551, https://doi.org/10.1093/neuros/nyaa453.
[34] D.G. Ellis, M. Garlinghouse, D.E. Warren, M.R. Aizenberg, Longitudinal changes in brain connectivity correlate with neuropsychological testing in brain tumor resection patients, Front. Neurosci. 19 (2025), https://doi.org/10.3389/fnins.2025.1532433.
[35] P.H. Luckett, M.O. Olufawo, K.Y. Park, et al., Predicting post-surgical functional status in high-grade glioma with resting state fMRI and machine learning, J. Neurooncol 169 (2024) 175–185, https://doi.org/10.1007/s11060-024-04715-1.
[36] V.M. Stoecklein, S. Stoecklein, F. Galiè, et al., Resting-state fMRI detects alterations in whole brain connectivity related to tumor biology in glioma patients, Neuro Oncol. 22 (2020) 1388–1398, https://doi.org/10.1093/neuonc/noaa044.
[37] K.-H. Nenning, J. Furtner, B. Kiesel, et al., Distributed changes of the functional connectome in patients with glioblastoma, Sci. Rep. 10 (2020) 18312, https://doi.org/10.1038/s41598-020-74726-1.
[38] M.E. Gurses, E. Gökalp, J. Spatz, et al., Augmented reality in cranial surgery: Surgical planning and maximal safety in resection of brain tumors via head-mounted fiber tractography, Clin. Neurol. Neurosurg. 251 (2025) 108820, https://doi.org/10.1016/j.clineuro.2025.108820.
[39] I.M. Young, N.B. Dadario, O. Tanglay, et al., Connectivity model of the anatomic substrates and network abnormalities in major depressive disorder: a coordinate meta-analysis of resting-state functional connectivity, J. Affect Disord. Rep. 11 (2023), https://doi.org/10.1016/j.jadr.2023.100478.
[40] H. Taylor, P. Nicholas, K. Hoy, et al., Functional connectivity analysis of the depression connectome provides potential markers and targets for transcranial magnetic stimulation, J. Affect Disord. 329 (2023), https://doi.org/10.1016/j.jad.2023.02.082.
[41] Y. Wang, J. Wang, W. Su, et al., Symptom-circuit mappings of the schizophrenia connectome, Psychiatry Res 323 (2023), https://doi.org/10.1016/j.psychres.2023.115122.
[42] H. Aerts, M. Schirner, T. Dhollander, et al., Modeling brain dynamics after tumor resection using The Virtual Brain, Neuroimage 213 (2020) 116738, https://doi.org/10.1016/j.neuroimage.2020.116738.